

Process-Integrated State Estimation of Optical Systems with Macro-micro Manipulators based on Wavefront Filtering

Christopher Schindlbeck, Christian Pape and Eduard Reithmeier

Abstract—To date, the assembly of optical systems is still not fully automated. Automated assembly can be facilitated by having an optical simulation at hand which, in turn, requires knowledge about the current state of the optical system. Due to the strict demands on the positioning tolerances, the uncertainties of the positioning system play an important role and lead to non-negligible deviations from the nominal poses. Therefore, the actual poses of the optical components need to be estimated in order to correct misaligned components. Furthermore, it is beneficial to develop methods that utilize the dedicated primary sensor and to avoid additional external sensors.

In this paper, we employ a macro-micro manipulator for moving optical components and utilize filtering methods to realize an in-process state estimation. For this, the uncertainty of the positioning system as well as sensor noise need to be identified which lay the groundwork for methods such as the Extended Kalman Filter, Iterated Extended Kalman Filter, Unscented Kalman Filter, or Particle Filter. In this paper, we compare these methods in simulation with current nonlinear approaches from literature with respect to the estimation error. Experimental verification is carried out by a macro-micro manipulator comprised of a Cartesian piezo-driven 3-DOF positioning system attached to a 6-DOF industrial robot. With the proposed filtering approach and macro-micro manipulator, the pose of a bi-convex lens is estimated via a wavefront sensor.

I. INTRODUCTION

Optical systems have many fields of application such as high-resolution length measurement or tactile-free surface reconstruction [1]. However, a fully automated solution for the assembly of optical systems does not exist yet. In general, such systems have strict demands on positioning tolerances. Placement of optical components in the assembly process is subject to the uncertainty of the (often specialized and expensive) positioning systems which are employed. Poor knowledge of the current state (i.e. the component poses) of the optical system impedes the applications of positional corrections to rectify the system during the assembly. This leads to fine-tuning of the optical components via active [2], [3] or passive [4], [5], [6] adjustment mechanisms after the assembly is completed.

Current state-of-the-art in optical system identification relies mostly on a nonlinear cost function based on Zernike coefficients [7], [8], [9]. The cost function can be minimized either via a gradient-free approach (NGF) approach, or by utilizing the gradient's information, via a gradient-based approach (NGB) approach [10]. Alternatively, neural networks [11]

can be used but the network needs to be trained again after altering the optical system (e.g. inserting a new component into the optical path). The aforementioned methods do not account for sensor noise and positioning uncertainty and the identification process might result in local minima due to the optical sensitivity [12]. Related work [13], [14] utilize an Iterated Extended Kalman Filter (IEKF) based on principal component analysis of a CCD sensor image to account for noise and uncertainty. To achieve a high-dimensional sensor decomposition, Karhunen-Loève modes are chosen therein. More recently, alternative sensors (so-called position sensitive devices [15]) are intentionally developed for the assembly of optical systems.

In this paper, we propose a method to obtain the current state of an optical system during the assembly process by employing a macro-micro manipulator and filtering techniques based on wavefront sensing. Macro-micro manipulators [16] (also micro-nano manipulators) combine the advantage of a large workspace of the macro system (here necessary for moving optical components) and precise local motion by a micro system (here for the identification of optical component's pose). In general, the field of application for such systems ranges from milling [17] to medical applications (minimally invasive surgery [18] or inner ear drug delivery [19]). Macro-micro manipulators utilizing optical signals as feedback for the assembly have been considered for example for packaging micro opto-electro-mechanical devices by visual servoing via a microscope camera [20]. However, therein, state estimation is not considered. Robotic systems in combination with a wavefront sensor have not been investigated yet for the estimation and assembly of optical systems. As methods for hand-eye calibration of wavefront sensors have not been developed yet, additional uncertainty is brought into the kinematics, which poses an additional challenge.

Over time, Bayesian estimation approaches have evolved as the method of choice for estimating the state of dynamic systems subject to noise [21]. If the noise is primarily assumed to be Gaussian, then Kalman filtering is preferred. On the other hand, if the noise is (primarily) non-Gaussian, the Particle Filter (PF) or the Gaussian sum filter are preferably used. In this case, better results might be achieved at the price of additional computational effort. Alternatively, an Unscented Kalman Filter (UKF) is expected to provide a balance between the low computational effort of the Kalman Filter (KF) and the high performance of the PF [22], [23]. These filtering approaches have generated an immense variety of submethods and the interested reader is referred to literature for an extensive overview on the numerous variants

All authors are with the Institute of Measurement and Automatic Control, Faculty of Mechanical Engineering, Leibniz Universität Hannover, 30167 Hanover, Germany, schindlbeck@imr.uni-hannover.de

of the KF [21], [24] or the PF [25]. These methods also find application in a large variety of core robotic tasks and have been extensively investigated in these contexts such as robot localization to estimate the state of mobile robotic platforms [26] or for estimating the geometrical parameters (positions, orientations and dimensions) of objects for manipulation tasks [27]. More examples for the application of filtering in robotics are given in [24].

For the optomechatronic state estimation, we will evaluate and compare four different filtering techniques in this paper: The Extended Kalman Filter (EKF), the IEKF, the UKF, and the PF. For filtering, the underlying probability distribution of the macro-micro manipulator positioning uncertainty as well as sensor noise need to be known or at least estimated. By performing repeated measurements and fitting Gaussian distributions to these, covariance matrices can be obtained which allow to find a process and noise model to enable the aforementioned state estimation with filtering techniques.

In this paper, a simple optical system will be utilized as demonstrator consisting of a laser, a bi-convex lens, and a wavefront sensor to validate our proposed approach. After the identification of process and sensor noise, the simulation is used to compare filtering methods with nonlinear approaches. Experimental verification is then carried out to estimate the pose of a lens between a laser and a wavefront sensor.

This paper is structured as follows. In Sec. II, optical preliminaries are given for uninitiated reader which lay the groundwork for the estimation approach. Sec. III outlines the proposed optomechatronic state estimator to obtain the current state of the optical system. In Sec. IV, we provide results from the identification of the process and measurement covariance matrices, simulation to test the approach against ground truth, and experimental results. Sec. V concludes the paper and gives a brief outlook.

II. OPTICAL PRELIMINARIES

In this section, a brief overview on the optical preliminaries (which is mostly adopted from [28], [29]) is given for readers unfamiliar with optics. These form the foundation for the upcoming sections.

A. Wavefronts & Zernike Polynomials

Wavefronts are defined as surfaces of equal phase (or multiples of 2π). It is possible to express any wavefront by a linear combination of so-called Zernike polynomials. Zernike polynomials are circular polynomials which are orthogonal over the unit disk. They can be conveniently expressed in polar coordinates by

$$Z_n^m(\rho, \theta) = \begin{cases} N_n^m R_n^m(\rho) \sin(m\theta) & \text{for } m < 0 \\ N_n^m R_n^m(\rho) \cos(m\theta) & \text{for } m \geq 0. \end{cases} \quad (1)$$

Therein, N_n^m is a normalization factor, R_n^m a radial polynomial, $0 \leq \rho \leq 1$ the normalized radial distance, and $0 \leq \theta \leq 2\pi$ the azimuthal angle. The integer n (polynomial

order) is nonnegative and the integer m (sinusoidal frequency) is chosen such that $n - |m|$ is even and nonnegative [30]. The radial Zernike polynomial $R_n^m(\rho)$ is defined as

$$R_n^m(\rho) = \sum_{k=0}^{(n-|m|)/2} \frac{(-1)^k (n-k)!}{k! \binom{n+|m|}{2-k}! \binom{n-|m|}{2-k}!} \rho^{n-2k}$$

and the normalization factor N_n^m is defined as

$$N_n^m = \sqrt{\frac{2(n+1)}{1+\delta_{m0}}}.$$

Therein, the Kronecker delta δ_{m0} is defined as

$$\delta_{m0} = \begin{cases} 1 & \text{for } m = 0 \\ 0 & \text{for } m \neq 0. \end{cases}$$

Noll's sequential indexing [31] facilitates the serial expansion of a wavefront by utilizing a single index ($Z_n^m \rightarrow Z_j$) for the Zernike polynomials. Following this single indexing scheme, we can expand the wavefront Φ in polar coordinates as

$$\Phi(\rho, \theta) = \sum_{j=1}^{n_z} z_j N_j Z_j(\rho, \theta) =: \mathbf{z}^T \mathbf{Z}(\rho, \theta). \quad (2)$$

Therein, the j -th Zernike coefficient z_j is associated with the j -th normalized polynomial $N_j Z_j$ which can be cast into vectorial form with a vector of Zernike coefficients $\mathbf{z} \in \mathbb{R}^{n_z}$ and normalized Zernike polynomials $\mathbf{Z} \in \mathbb{R}^{n_z}$. A list of the first ten Zernike polynomials (which are later utilized in the simulation and experiment in Sec. IV) with their corresponding common names is given in Tab. I.

B. Shack-Hartmann Sensor

A Shack-Hartmann sensor (see Fig. 1 for a schematic depiction of the working principle) is capable of reconstructing wavefronts. An incoming wavefront is projected to a CCD sensor with the help of a microlens array. A planar wavefront will form dots at the sensor plane which are centered w.r.t. their microlenses. If the wavefront is not planar, displacements of the formed dots from their nominal center occur. From the dot displacements, it is possible to reconstruct the wavefront with a least-squares optimization procedure [32].

For the remainder of the paper, we will only use the Zernike coefficients \mathbf{z} to describe the wavefront since they allow for a concise and complete description.

III. OPTICAL STATE ESTIMATION

This section presents the theoretical ground work for the state estimation of optical systems with the help of a mechatronic positioning system.

A. State-space Equations

The overall system can be written in state-space form as

$$\dot{\mathbf{x}} = \mathbf{f}(\mathbf{x}, \mathbf{u}) + \mathbf{w} \quad (3)$$

$$\mathbf{z} = \mathbf{h}(\mathbf{x}) + \mathbf{v} \quad (4)$$

TABLE I: Utilized Zernike polynomials with corresponding coefficients, normalization factors, and common names ordered by Noll's sequence.

Zernike coefficient z_j	n	m	Normalization factor N_n^m	Zernike polynomial $Z_j = Z_n^m(\rho, \theta)$	Common name
z_1	0	0	1	1	Piston
z_2	1	1	2	$\rho \cos(\theta)$	Tip
z_3	1	-1	2	$\rho \sin(\theta)$	Tilt
z_4	2	0	$\sqrt{3}$	$2\rho^2 - 1$	Defocus
z_5	2	-2	$\sqrt{6}$	$\rho^2 \sin(2\theta)$	Oblique astigmatism
z_6	2	2	$\sqrt{6}$	$\rho^2 \cos(2\theta)$	Vertical astigmatism
z_7	3	-1	$2\sqrt{2}$	$(3\rho^3 - 2\rho) \sin(\theta)$	Vertical coma
z_8	3	1	$2\sqrt{2}$	$(3\rho^3 - 2\rho) \cos(\theta)$	Horizontal coma
z_9	3	-3	$2\sqrt{2}$	$\rho^3 \sin(3\theta)$	Vertical trefoil
z_{10}	3	3	$2\sqrt{2}$	$\rho^3 \cos(3\theta)$	Oblique trefoil

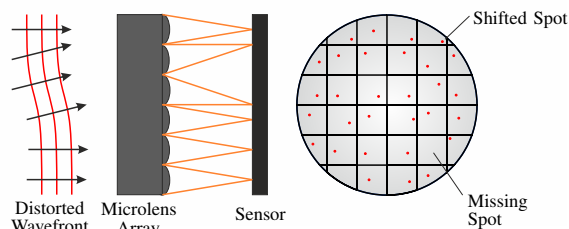


Fig. 1: Schematic depiction of Shack-Hartmann sensor working principle. Incoming distorted wavefront maps to dot displacements from their nominal center.

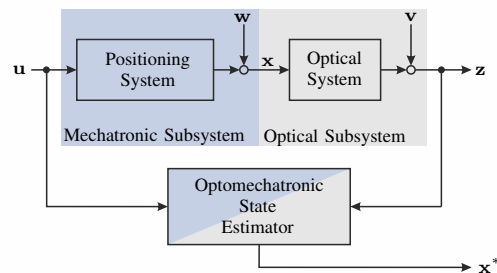


Fig. 2: Block diagram for optomechatronic state estimator.

and is comprised of a mechatronic (3) and an optical subsystem (4). The mechatronic system is a positioning device (e.g. robotic system, Cartesian manipulator) driven by a control input $\mathbf{u} \in \mathbb{R}^{n_u}$ capable of positioning optical components described by the pose vector $\mathbf{x} \in \mathbb{R}^{n_x}$. Therein, n_u and n_x denote the degrees of freedom (DOF) of the positioning device and the optical components, respectively. The device is subject to positioning uncertainty $\mathbf{w} \in \mathbb{R}^{n_x}$ which can be assumed to be additive and normally distributed with zero mean and covariance matrix \mathbf{Q} , i.e. $\mathbf{w} \sim \mathcal{N}(\mathbf{0}, \mathbf{Q})$.

The optical subsystem consists of a (fixed) light source, optical components, and a (fixed) wavefront sensor¹. In this paper, we assume that the optical properties of the components are known with sufficient accuracy such that the output of the optical system solely depends on the pose of its components. The sensor returns a vector of Zernike coefficients $\mathbf{z} \in \mathbb{R}^{n_z}$ (see Sec. II) and is subject to sensor noise $\mathbf{v} \in \mathbb{R}^{n_z}$. Again, the sensor noise can also be assumed to be additive, zero mean and normally distributed described by a covariance matrix \mathbf{R} , i.e. $\mathbf{v} \sim \mathcal{N}(\mathbf{0}, \mathbf{R})$.

In this paper, we assume that the positioning system is feedback-controlled and tuned such that steady-state errors are eliminated over time. The transient response only plays a minor role in the placement of objects due to small time constants compared to the entire assembly process. Therefore, the state equation can be described by a linear

input-output relation. The discrete-time state-space equations then result in

$$\mathbf{x}_{k+1} = \mathbf{A}_k \mathbf{x}_k + \mathbf{B}_k \mathbf{u}_k + \mathbf{w} \quad (5)$$

$$\mathbf{z}_k = \mathbf{h}(\mathbf{x}_k) + \mathbf{v}. \quad (6)$$

In this paper, we assume that $\mathbf{A}_k = \mathbf{A} = \mathbf{I}$ and $\mathbf{B}_k = \mathbf{B} = \mathbf{I}$, meaning that undesired cross-coupling disturbances are neglected and should be handled by the controller and the state-space matrices are time-invariant. The goal of this paper is to estimate the optical component poses i.e. the state \mathbf{x} . Fig. 2 shows that optical component poses cannot be directly obtained and therefore this has to be achieved through means of state estimation.

B. State Estimation

Although the measurement equation (6) has non-negligible nonlinearities, which need to be considered, it is still useful to have local information around the operating point. Sensitivity analysis studies the local impact of input changes (here: optical component poses) to output changes (here: Zernike coefficients). In general, as there is no analytic description of \mathbf{h} , the sensitivity matrix $\mathbf{S} \in \mathbb{R}^{n_z \times n_x}$ (the Jacobian) needs to be found via numerical differentiation. Since a discrete-time representation is chosen here, the sensitivity matrix $\mathbf{S}_k \approx \partial \mathbf{h}(\mathbf{x}_k) / \partial \mathbf{x}_k$ is dependent on the discrete time step and needs to be updated for each time step. Sensitivity analysis also provides insight into the difficulty of state estimation. Especially ill-conditioned sensitivity matrices will directly lead to the deterioration of the estimation accuracy [33].

In general, it is not guaranteed that all states can be reconstructed from measurements alone. To ensure the feasibility

¹The restriction of a fixed light source and sensor is without loss of generality but simplifies the demonstrator assembly significantly.

of state estimation, observability needs to be ensured [34]. By linearization of the measurement equation (4) via the sensitivity matrix \mathbf{S}_k , a discrete-time linear time-variant system is obtained. For such systems, (total) observability is achieved if the observability matrix

$$\mathcal{O}_{k_0} = \begin{bmatrix} \mathbf{S}_{k_0} \\ \mathbf{S}_{k_0+1} \mathbf{A}_{k_0} \\ \mathbf{S}_{k_0+2} \mathbf{A}_{k_0+1} \mathbf{A}_{k_0} \\ \vdots \\ \mathbf{S}_{k_0+n-1} \mathbf{A}_{k_0+n-2} \cdots \mathbf{A}_{k_0+1} \mathbf{A}_{k_0} \end{bmatrix} \quad (7)$$

has full rank (for any initial time k_0) [35].

It should be noted that wavefront sensors are able to provide a large number of Zernike coefficients as compared to the DOF of the state to be estimated. Therefore, $n_z \gg n_x$ holds in practical applications. Since the measurement equation (6) is time-variant, this condition needs to be evaluated after each filter iteration in Sec. IV.

The corresponding dual problem to observability is (state) controllability. In this paper, this condition is trivially satisfied at all times since the optical system is placed far from the boundaries of the workspace where certain DOF cannot be controlled anymore by the macro-micro manipulator system. In this paper, four well-known filtering techniques are employed, the EKF, the IEKF, the UKF, and the PF. The specific implementation details for the simulation and experiments can be found in Sec. IV-C.

IV. SIMULATION AND EXPERIMENTAL RESULTS

This section describes the experimental setup, the results from the identification of the process and measurement covariance matrices and presents the results of the simulation and experiment. The optical system is deliberately chosen to be simple in order to validate the state estimation approach. However, the identification process can be repeated in a straightforward manner for each (additional) optical component to be assembled which allows the integration into more complex assembly procedures [12].

A. Experimental Setup

The macro-micro manipulator utilized for the experiment is comprised of an industrial robot, a piezo-driven micro-positioning unit, and a gripper. The industrial robot is a KUKA Agilus KR10R1100 sixx manipulator with six DOF. It has a closed control architecture and the desired poses are commanded via ROS [36]. Attached to the industrial robot is a piezo-driven micro-positioning unit with three DOF that is PID voltage-controlled [17]. The voltage is converted to Cartesian displacement with the calibration data provided by the manufacturer. The load-free maximum displacement is 200 μm in each axis. The micro-positioning unit can take commands via ROS which are passed to LabView running on a real-time system. Then, an amplifier converts the signals to the piezoelectric actuators and from the strain-gauge sensors accordingly. Furthermore, a gripper is attached to the micro-positioning unit to pick, place and hold mounted optical components.

The optical system consists here of a laser (green, $\lambda = 532 \text{ nm}$), a single optical component (a bi-convex lens with 50 mm focal length), and a wavefront sensor (Thorlabs WFS150-5C with a 150 μm microlens array pitch). This wavefront sensor is capable of providing up to 66 Zernike coefficients. In this paper, we use the first nine Zernike coefficients ($n_z = 9$, without piston) for the state estimation. Since the lens is rotationally symmetric around its z -axis, only five DOF can be observed. The conclusion can be drawn from evaluating the rank of the observability matrix (7). Therefore, we reduce the state vector to the number of observable states, i.e. $n_x = 5$. The wavefront sensor is interfaced via LabView which processes the raw sensor data and then passes the Zernike coefficients to MATLAB where the state estimation is implemented. The experimental setup is depicted in Fig. 3.

B. Identification of Process and Measurement Noise

In order to implement/improve converge of the filtering approaches, the Cartesian covariance matrices need to be known/estimated.

a) *Macro-micro manipulator*: For the industrial robot, the (reduced) Cartesian covariance matrix is $\mathbf{Q}_M = \text{diag}(\sigma_{M,x}^2, \sigma_{M,y}^2, \sigma_{M,z}^2, \sigma_{M,\theta_x}^2, \sigma_{M,\theta_y}^2)$. Therein, cross-coupling effects are neglected and only the five DOF to fully identify the lens pose are considered. Since neither accuracy nor repeatability is disclosed for most industrial robotic systems, a laser tracker has been used to find the repetition accuracy. By obtaining measurements after repeated positioning, the standard deviations are found to be $\sigma_{M,x} = 0.1500 \text{ mm}$, $\sigma_{M,y} = 0.0778 \text{ mm}$, $\sigma_{M,z} = 0.2189 \text{ mm}$, $\sigma_{M,\theta_x} = 0.0210^\circ$, and $\sigma_{M,\theta_y} = 0.0195^\circ$.

The covariance matrix of the micro-positioning unit \mathbf{Q}_m contains the standard deviations of the three Cartesian DOF of the micro-positioning unit. Hence, the covariance matrix has the structure $\mathbf{Q}_m = \text{diag}(\sigma_{m,x}^2, \sigma_{m,y}^2, \sigma_{m,z}^2, 0, 0)$. Here, repetition accuracy is again found by repeated positioning, measuring strain-gauge output and converting it to Cartesian displacement via calibration data provided by the manufacturer. We find the standard deviations to be $\sigma_{m,x} = 0.3657 \mu\text{m}$, $\sigma_{m,y} = 0.4572 \mu\text{m}$, and $\sigma_{m,z} = 0.5255 \mu\text{m}$.

b) *Wavefront sensor*: For the identification of the measurement covariance matrix, continuous measurements from the wavefront sensor are obtained. For this, the lens was placed inside the optical path to get comparable results for the simulation and experiment. Now, the mean value and standard deviation for each Zernike coefficient can be obtained by fitting the data to a Gaussian distribution. The mean values are non-zero since the lens is inside the optical path resulting in a convex-shaped wavefront. For the covariance measurement matrix $\mathbf{R} = \text{diag}(\sigma_{z,1}^2, \sigma_{z,2}^2, \dots, \sigma_{z,n_z}^2)$, only the standard deviations are of interest. Cross-talk between Zernike coefficients can be neglected in this paper as only lower-order aberrations are considered which exhibit minimal cross-correlation. Fig. 4 shows the distribution of two Zernike coefficients (after mean value subtraction) and

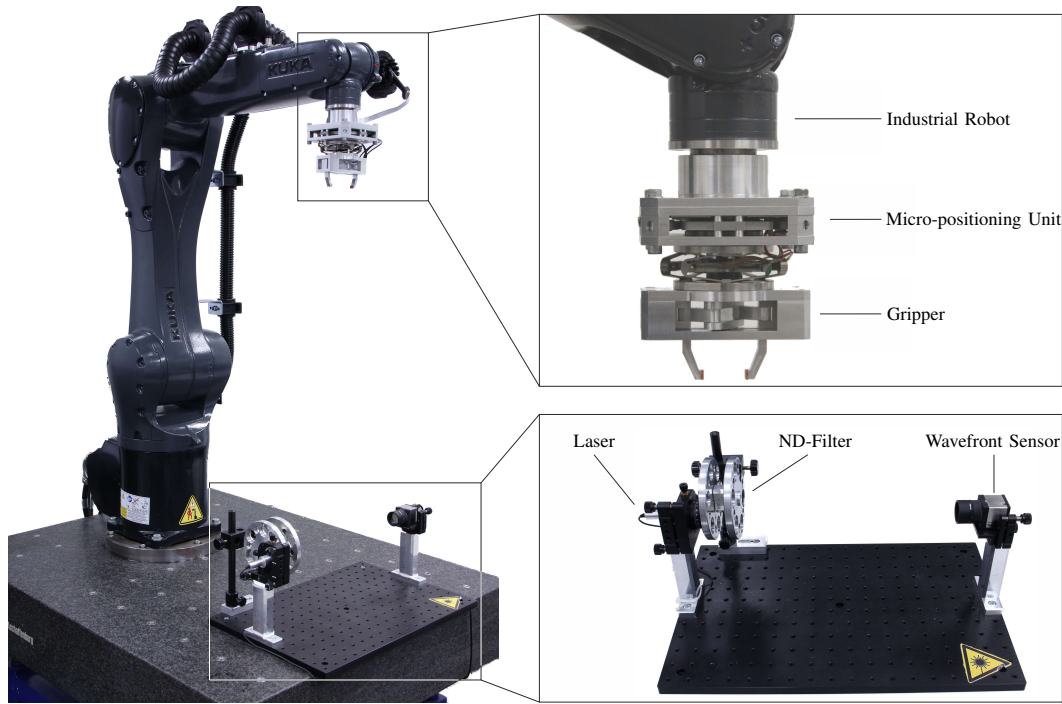


Fig. 3: Setup with macro-micro manipulator and optical system utilized in the experiment. The macro-micro manipulator is comprised of an industrial robot and a micro-positioning unit. Additionally, a gripper is attached to the micro-positioning unit for object handling. The optical setup is shown without any optical components.

the corresponding fit. Tab. II lists all ten mean values and standard deviations of the Zernike coefficients utilized in the simulation and experiment.

TABLE II: Identified mean and standard deviations of Zernike coefficients obtained from sensor data.

Zernike Coefficient	$\mu_z / \mu\text{m}$	$\sigma_z / \mu\text{m}$
z_1 (Piston)	1.0894	0.0289
z_2 (Tip)	0.2205	0.0202
z_3 (Tilt)	0.5336	0.0147
z_4 (Defocus)	-1.8092	0.0052
z_5 (Oblique astigmatism)	-0.0015	0.0077
z_6 (Vertical astigmatism)	0.0122	0.0080
z_7 (Vertical coma)	-0.0021	0.0051
z_8 (Horizontal coma)	-0.0253	0.0037
z_9 (Vertical trefoil)	-0.0150	0.0045
z_{10} (Oblique trefoil)	-0.0026	0.0046

C. Simulation

In order to find the approach that yields the most accurate results, the proposed state estimator is tested against ground truth in simulation first. For the filtering approaches, the identification results of section IV-B will be used. Since the industrial robot will insert the component in the optical train, the initial covariance matrix corresponds to the positioning uncertainty of the macro-positioning system $\mathbf{Q}_0 = \mathbf{Q}_M$. In this paper, we follow a decoupled approach for the generation of identification trajectories to mitigate cross-coupling effects, i.e. the macro system (here: the industrial robot) and the micro-positioning unit will not move simultaneously. The macro system will move along the less sensitive direction,

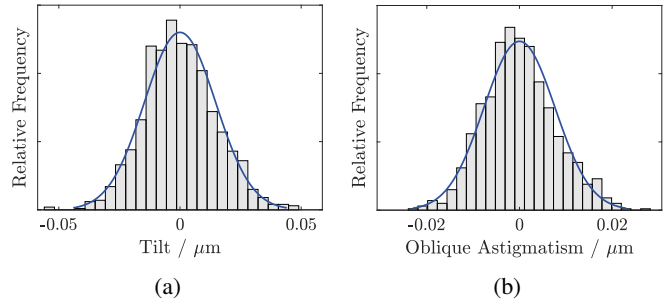


Fig. 4: Selected Zernike coefficients (after mean value subtraction) from recorded sensor data (gray) with normal distribution fit (blue): Tilt z_3 (a) and oblique astigmatism z_5 (b).

where larger ranges of motion and less precision is required. The micro system (the piezo-driven micro-positioning unit) will move the system along higher sensitive directions. This requires shorter ranges of motion with higher repeatability.

For the bi-convex lens employed in the simulation and experiment, the directions with low sensitivity are z , θ_x , and θ_y and directions with high sensitivity are x and y [12].

Fig. 5a depicts the actual state of the lens during simulation. The initial state is different from zero due to the positioning uncertainty. Then, trajectories are executed which are symmetrical around zero and the range of motion in each axis is proportional to the sensitivity in this direction. As long as the sensor is sufficiently illuminated, trajectories with a large displacement range should be chosen. Furthermore, it shows

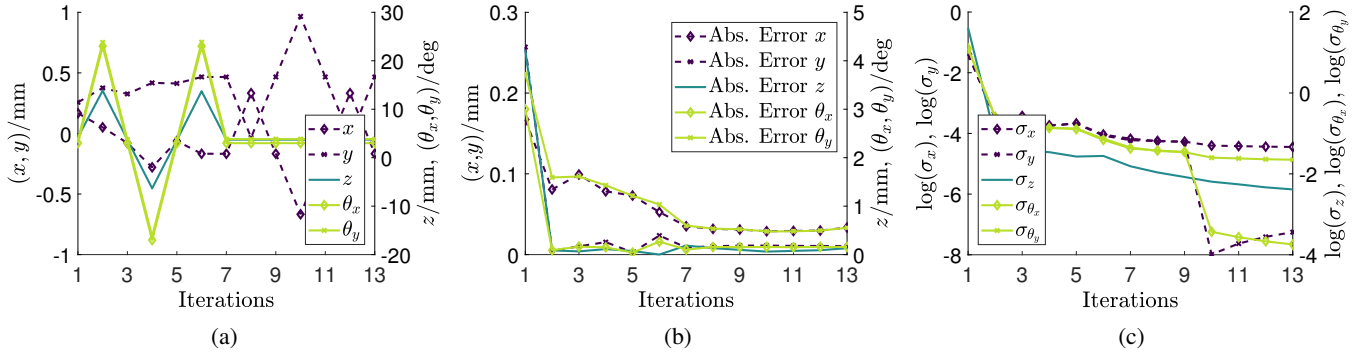


Fig. 5: True state (ground truth) of the optical component (a), absolute identification error (b), and logarithmic plot of the standard deviation of the state covariance matrix for the EKF.

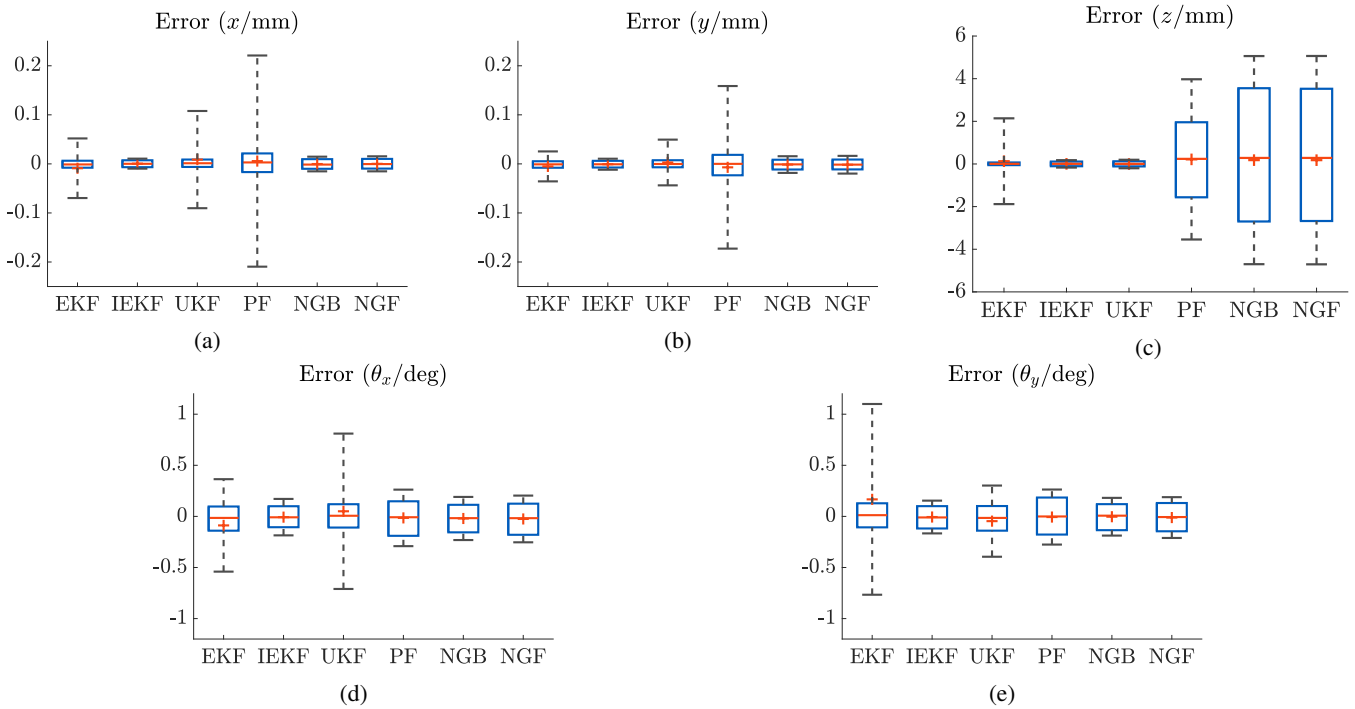


Fig. 6: Box plots of error in x -, y -, z -, θ_x -, and θ_y -direction for different filtering (EKF, IEKF, UKF, PF) and nonlinear optimization (NGB, NGF) approaches. The data was obtained after 300 trials. The median is indicated by —, the mean value μ by +, the interquartile range by —, and the 9th/91st percentile by the whiskers —.

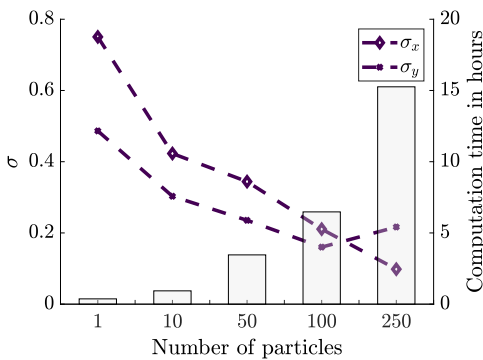


Fig. 7: Impact of the chosen number of particles on standard deviations of x , y , and resulting computation time.

that first the macro system is moved and then the micro-positioning unit. Fig. 5b depicts the absolute estimation error $|e_k| = |k - k^*|$ for each state $k \in \{x, y, z, \theta_x, \theta_y\}$ with an EKF, where imminent estimation improvement can be observed. Fig. 5c shows the standard deviation obtained from the state covariance matrix. After iteration seven, the micro-positioning unit moves which drives down the estimation uncertainty in y - and θ_x -direction.

In order to compare different strategies for estimating the optical component pose, Tab. III lists three approaches and its effect on the estimation accuracy. Moving the optical component with the macro system first and then the micro-positioning unit is denoted by Mm. Conversely, moving the micro-positioning unit first and then the macro system is denoted by mM. Strategy m denotes that only the micro-

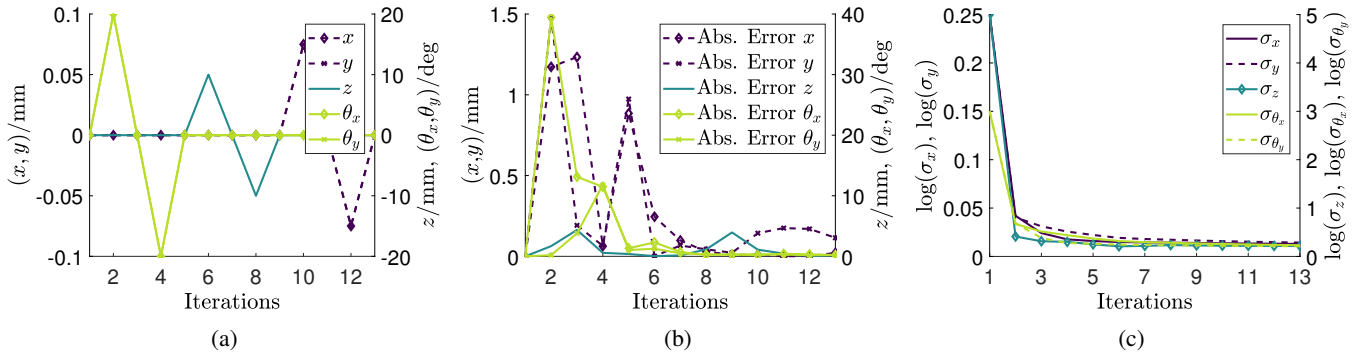


Fig. 8: Results of the estimation experiment with the IEKF. In (a), the nominal trajectory is shown while (b) shows the error between predicted and corrected states obtained from the optomechatronic state estimator. (c) shows the standard deviation obtained from diagonal entries of of the corrected state covariance matrix.

TABLE III: Mean, median, and standard deviation (Sd) of the identification error obtained in all 5 directions after 200 trials with an EKF for three strategies (Mm, mM, and m). For better comparability, the smallest values of the standard deviation are highlighted in color.

Dir.		Mm	mM	m
x	Mean	$-8.99 \cdot 10^{-3}$	$4.25 \cdot 10^{-2}$	$4.37 \cdot 10^{-3}$
	Median	$-1.90 \cdot 10^{-3}$	$9.02 \cdot 10^{-3}$	$1.34 \cdot 10^{-2}$
	Sd	$5.66 \cdot 10^{-2}$	$2.70 \cdot 10^{-1}$	$1.02 \cdot 10^{-1}$
y	Mean	$2.58 \cdot 10^{-3}$	$2.76 \cdot 10^{-3}$	$-6.25 \cdot 10^{-3}$
	Median	$5.72 \cdot 10^{-4}$	$4.65 \cdot 10^{-3}$	$-5.43 \cdot 10^{-3}$
	Sd	$5.97 \cdot 10^{-2}$	$7.37 \cdot 10^{-2}$	$1.11 \cdot 10^{-1}$
z	Mean	$1.45 \cdot 10^{-2}$	$1.63 \cdot 10^{-2}$	$6.88 \cdot 10^{-2}$
	Median	$2.21 \cdot 10^{-2}$	$7.26 \cdot 10^{-7}$	$7.45 \cdot 10^{-2}$
	Sd	$1.46 \cdot 10^{-1}$	$2.98 \cdot 10^{-1}$	$1.55 \cdot 10^{-1}$
θ_x	Mean	$4.07 \cdot 10^{-2}$	$4.02 \cdot 10^{-2}$	$-1.01 \cdot 10^{-1}$
	Median	$5.16 \cdot 10^{-3}$	$7.01 \cdot 10^{-2}$	$-9.59 \cdot 10^{-2}$
	Sd	$9.75 \cdot 10^{-1}$	1.19	1.81
θ_y	Mean	$1.47 \cdot 10^{-1}$	$-1.11 \cdot 10^{-1}$	$-7.15 \cdot 10^{-2}$
	Median	$5.16 \cdot 10^{-2}$	$-1.47 \cdot 10^{-1}$	$2.47 \cdot 10^{-1}$
	Sd	$9.27 \cdot 10^{-1}$	1.18	1.66

positioning unit in its three Cartesian DOF is moved. By looking at the standard deviation after 200 trials, the Mm strategy yields the smallest value. Roughly speaking, one can gain an order of magnitude in estimation accuracy by following a macro-micro manipulator approach. In particular, the directions with high sensitivity (here x, y) benefit from this approach.

D. Statistical Comparison

For a thorough evaluation of the proposed methods, statistical analysis is necessary due to the underlying stochastic nature of the uncertainties. We conduct repeated trials to compare the estimation accuracy of the filtering methods from Sec. III-B with common nonlinear approaches based on a quadratic cost function [12], [10]. The obtained minimum of the cost function then yields the estimated pose. In this paper, we use a quasi-Newton algorithm as an NGB approach and a simplex search method as NGF approach. For the UKF, the sigma points are chosen here based on the unscented transformation which is parameterized by α , β , and κ . α is a scaling parameter determining the spread of the sigma

points, κ a secondary scaling parameter usually set to zero, and β is used to incorporate prior knowledge of the state distribution. In this paper, we choose $\beta = 0$ which is optimal for Gaussian distributions and the remaining scaling parameters to be $\alpha = 10^{-3}$ and $\kappa = 0$ [37]. For the IEKF, we implemented the variable step-length line search IEKF [38] with 20 maximum iterations and a minimum step size $\alpha_{iekf,max} = 10^{-8}$. The PF implemented in this paper uses a mean state estimation method and a multinomial resampling method with 100 particles.

Fig. 6 depicts the box plots of the estimation error for 300 trials. For axial displacement of the lens, filtering approaches outperform nonlinear approaches. For lateral displacements and tilts, the data within in the interquartile range are in same order of magnitude. However, the EKF, the UKF, and the PF spread the data over a wider range (indicated by the whiskers). For the IEKF, the 9th/91st percentile is always close to the interquartile range indicating higher estimation accuracy. Furthermore, the EKF (and the UKF to some extent) appears to produce a systematic bias when estimating tilt indicating a preferred estimation direction. For the IEKF, on the other hand, mean and median values are always close to each other. While the PF appears to be inferior in the quality of lateral estimation, given enough computational resources, the PF should match or surpass the performance of the other approaches. Fig. 7 shows the influence of the number of particles on the achievable accuracy and computation time. However, due to this high computational load, the PF becomes impractical for optical pose estimation in assembly scenarios. Similar results have already been observed for robotic pose estimation [39]. The type of nonlinear optimization does not seem to affect the estimation accuracy. In conclusion, the IEKF consistently yielded the highest estimation accuracy for all states. However, this means that longer computation times as compared to the EKF and UKF have to be taken into consideration.

E. Experimental Results

For the experiment, the strategy which had the best performance in simulation will be chosen, which is an IEKF and by moving the macro-manipulator first and then the micro-

positioning unit (see Tab. III). Fig. 8a shows the nominal trajectory that has been commanded to the macro-micro manipulator via respective control inputs to the industrial robot and micro-positioning unit. As the true state of the optical component is unknown, experimental results do not provide ground truth for the evaluation of the estimation error. Instead, the absolute error between predicted and corrected states and the standard deviations from the state covariance matrix are shown in Fig. 8b and 8c, respectively. In general, smaller values indicates a higher confidence in the estimate.

V. CONCLUSION AND FUTURE WORK

In this paper, an optomechatronic state estimator has been presented to infer optical component poses via a wavefront sensor. A macro-micro manipulator has been employed which on the one hand is able to grasp and move optical components near the optical system due to its large workspace and on the other hand the micro-positioning unit is able to fine-adjust optical components. The statistical simulation results show that filtering approaches are superior to nonlinear approaches and generally lead to a smaller estimation error. Further, the strategy to move a lens first by the macro system and then by the micro system resulted in a smaller standard deviation of the estimation error compared to other strategies. Experimental validation has been executed and the convergence of the predicted and corrected states could be observed.

For future work, simultaneous identification of the optical component poses as well as its optical parameters or even geometric properties should be addressed. Furthermore, as an alternative to the filtering methods of the presented optomechatronic state estimator, batch estimation methods could also be analyzed. Also, trajectory synthesis for persistent excitation is a topic that needs a dedicated analysis for this application.

REFERENCES

- [1] W. Singer, M. Totzeck, and H. Gross, *Handbook of Optical Systems, Volume 2: Physical Image Formation*. John Wiley & Sons, 2006.
- [2] D. R. Neal and J. Mansell, "Application of shack-hartmann wavefront sensors to optical system calibration and alignment," in *Proc. Workshop on AOIM*, 2000, pp. 234–243.
- [3] R. E. Abbink, "Interferometer alignment," 2005, US Patent 6,952,266.
- [4] F. Acernese, P. Amico, M. Al-Shourbagy, S. Aoudia *et al.*, "The virgo automatic alignment system," *Classical and Quantum Gravity*, vol. 23, no. 8, p. S91, 2006.
- [5] A. Cenko, "Automatic interferometric alignment of a free-space optical coherence tomography system," Ph.D. dissertation, University of Waterloo, 2011.
- [6] D. Kalamatianos, P. E. Wellstead, J. M. Edmunds, and P. Liatsis, "Active alignment for two-beam interferometers," *Review of Scientific Instruments*, vol. 77, no. 1, p. 013103, 2006.
- [7] E. D. Kim, Y.-W. Choi, M.-S. Kang, and S. C. Choi, "Reverse-optimization alignment algorithm using zernike sensitivity," *J. Opt. Soc. Korea*, vol. 9, no. 2, pp. 68–73, 2005.
- [8] S. Kim, H.-S. Yang, Y.-W. Lee, and S.-W. Kim, "Merit function regression method for efficient alignment control of two-mirror optical systems," *Optics Express*, vol. 15, no. 8, pp. 5059–5068, 2007.
- [9] H.-S. Yang, S.-H. Kim, Y.-W. Lee, J.-B. Song, H.-G. Rhee, H.-Y. Lee, J.-H. Lee, I.-W. Lee, and S.-W. Kim, "Computer aided alignment using zernike coefficients," in *Proc. of SPIE Vol. 6293*, 2006, p. 62930I.
- [10] C. Schindlbeck, C. Pape, and E. Reithmeier, "Wavefront predictions for the automated assembly of optical systems," Y. Wang, T. E. Kidger, and K. Tatsuno, Eds., vol. 10815, 2018, pp. 10815–108157.
- [11] F. Z. Adil, E. İ. Konukseven, T. Balkan, and Ö. F. Adil, "Optical alignment procedure utilizing neural networks combined with shack-hartmann wavefront sensor," *Opt. Eng.*, vol. 56, no. 5, pp. 051402–051402, 2017.
- [12] C. Schindlbeck, C. Pape, and E. Reithmeier, "Predictor-corrector framework for the sequential assembly of optical systems based on wavefront sensing," *Optics Express*, vol. 26, pp. 10669–10681, 2018.
- [13] J. Fang and D. Savransky, "Automated alignment of a reconfigurable optical system using focal-plane sensing and kalman filtering," *Applied Optics*, vol. 55, no. 22, pp. 5967–5976, 2016.
- [14] —, "Model-based estimation and control for off-axis parabolic mirror alignment," in *Photonic Instrumentation Engineering V*, vol. 10539. SPIE, 2018, p. 105390X.
- [15] I. A. Ivan, M. Ardeleanu, G. J. Laurent, N. Tan, and C. Clevy, "The metrology and applications of psd (position sensitive detector) sensors for microrobotics," in *IEEE ISOT*, 2012.
- [16] A. Sharon and D. Hardt, "Enhancement of robot accuracy using endpoint feedback and a macro-micro manipulator system," in *IEEE American Control Conference*, 1984, pp. 1836–1845.
- [17] C. Schindlbeck, A. Janz, C. Pape, and E. Reithmeier, "Increasing milling precision for macro-micro-manipulators with disturbance rejection control via visual feedback," in *IEEE/RSJ IROS*, 2017, pp. 4686–4693.
- [18] S. Konishi, M. Nokata, O. C. Jeong, S. Kusuda, T. Sakakibara, M. Kuwayama, and H. Tsutsumi, "Pneumatic micro hand and miniaturized parallel link robot for micro manipulation robot system," in *Proc. of IEEE ICRA*, 2006, pp. 1036–1041.
- [19] W. Amokrane, K. Belharet, M. Souissi, A. B. Grayeli, and A. Ferreira, "Macro-micro manipulation platform for inner ear drug delivery," *Robotics and Autonomous Systems*, 2018.
- [20] R. Murthy, A. N. Das, D. Popa, and H. Stephanou, "M3: Multiscale, deterministic and reconfigurable macro-micro assembly system for packaging of mems," in *Proc. IEEE ICRA*, 2007, pp. 668–673.
- [21] H. Fang, N. Tian, Y. Wang, M. Zhou, and M. A. Haile, "Nonlinear bayesian estimation: from kalman filtering to a broader horizon," *IEEE/CAA J. Automatica Sinica*, vol. 5, no. 2, pp. 401–417, 2018.
- [22] A. Sitz, U. Schwarz, J. Kurths, and H. U. Voss, "Estimation of parameters and unobserved components for nonlinear systems from noisy time series," *Physical Review E*, vol. 66, no. 1, p. 016210, 2002.
- [23] D. Simon, *Optimal State Estimation: Kalman, H Infinity, and Nonlinear Approaches*. John Wiley & Sons, 2006.
- [24] S. Chen, "Kalman filter for robot vision: a survey," *IEEE Transactions on Industrial Electronics*, vol. 59, no. 11, pp. 4409–4420, 2012.
- [25] X. Wang, T. Li, S. Sun, and J. Corchado, "A survey of recent advances in particle filters and remaining challenges for multitarget tracking," *Sensors*, vol. 17, no. 12, p. 2707, 2017.
- [26] S. Thrun, "Robotic mapping: A survey," *Exploring artificial intelligence in the new millennium*, vol. 1, no. 1-35, p. 1, 2002.
- [27] T. Lefebvre, H. Bruyninckx, and J. Schutter, *Nonlinear Kalman filtering for force-controlled robot tasks*. Springer, 2005, vol. 19.
- [28] D. Malacara, *Optical Shop Testing*. John Wiley & Sons, 2007, vol. 59.
- [29] B. E. Saleh, M. C. Teich, and B. E. Saleh, *Fundamentals of Photonics*. Wiley New York, 1991, vol. 22.
- [30] Y. Xin, M. Pawlak, and S. Liao, "Accurate computation of zernike moments in polar coordinates," *IEEE Trans. Image Proc.*, vol. 16, no. 2, pp. 581–587, 2007.
- [31] R. J. Noll, "Zernike polynomials and atmospheric turbulence," *J. Opt. Soc. Am.*, vol. 66, no. 3, pp. 207–211, 03 1976.
- [32] R. Cubalchini, "Modal wave-front estimation from phase derivative measurements," *JOSA*, vol. 69, no. 7, pp. 972–977, 1979.
- [33] L. E. Olivier, B. Huang, and I. K. Craig, "Dual particle filters for state and parameter estimation with application to a run-of-mine ore mill," *Journal of Process Control*, vol. 22, no. 4, pp. 710–717, 2012.
- [34] K. S. Tsakalis and P. A. Ioannou, *Linear time-varying systems: control and adaptation*. Prentice-Hall, Inc., 1993.
- [35] M. Witczak, V. Puig, D. Rotondo, and P. Witczak, "A necessary and sufficient condition for total observability of discrete-time linear time-varying systems," *IFAC-PapersOnLine*, vol. 50, no. 1, pp. 729–734, 2017.
- [36] S. Edwards and C. Lewis, "Ros-industrial: applying the robot operating system (ros) to industrial applications," in *IEEE IROS, ECHORD Workshop*, 2012.

- [37] E. A. Wan and R. Van Der Merwe, "The unscented kalman filter for nonlinear estimation," in *Proc. IEEE AS-SPCC Symposium*, 2000, pp. 153–158.
- [38] J. Havlík and O. Straka, "Performance evaluation of iterated extended kalman filter with variable step-length," in *Journal of Physics: Conference Series*, vol. 659, no. 1. IOP Publishing, 2015, p. 012022.
- [39] P. Furgale, T. D. Barfoot, and G. Sibley, "Continuous-time batch estimation using temporal basis functions," in *Proc. IEEE IROS*, 2012, pp. 2088–2095.